Simulation of Photonic Crystals based on silicon nanopillars

Author: Zoilo Núñez Lasús.
*Facultat de Física, Universitat de Barcelona, Diagonal 645, 08028 Barcelona, Spain.**

Advisors: Elena López Aymerich and Albert Romano Rodriguez.

Abstract: In this work we study the properties of 2D photonic crystals based on silicon nanopillars through electromagnetic simulations via the finite-difference time-domain method. Bandgaps will be analyzed through transmission spectra across different configurations and defects introduced in the structure in visible and near-infrared regions. An optimal bandgap size is found in terms of gap-midgap for an specific radius-to-pitch ratio. Additionally a modified waveguide is studied, showing a ressonance peak which can be used as a narrow-band filter.

I. INTRODUCTION

Controlling the way light propagates through materials has been a growing field of interest in the last decades. Photonic crystals (PC) have emerged as a popular solution, a periodic dielectric medium which can forbid the light propagation in certain directions and at frequencies within a certain range, the photonic band gap (PBG). The manipulation of these periodic structures by changing the distribution of dielectric material or introducing local defects [1] have provided multiple applications in optoelectronics, such as lasers, filters or solar cells [2]. The simulation of these photonic crystals has turned then into a particularly useful feature in the designing process, providing background information prior to manufacturing. Thus, numerical methods, such as the finite-difference time-domain (FDTD) method [3], are widely used to compute numerical solutions of Maxwell's equations in the research process of photonic crystals properties and applications.

The aim of this work is then, to carry out extensive simulations, using the FDTD method, of photonic crystals formed by silicon nanopillars distributed in an hexagonal lattice, which has proven to produce a broad PBG [5], while discussing its dependance with geometrical and topological parameters. Besides, defects will be introduced in the structures while considering the results obtained for further manufacturing processes.

II. COMPUTATIONAL METHODS

To solve Maxwell equations, the FDTD method will discretize space and time into a rectangular grid following the Yee's algorithm [3], where time dependent components of the electromagnetic field will be computed by central-difference approximation.

The band gaps will be calculated by analyzing the transmittance and reflectance spectra. Therefore, we shall compute the transmitted power P through the structure, which is the integral of the Poynting vector in the $\hat{n}$ direction, over a plane given a single frequency w, as follows:

$$P(\omega) = \mathrm{Re}\,\hat{\mathbf{n}} \cdot \int \mathbf{E}_\omega(\mathbf{x})^* \times \mathbf{H}_\omega(\mathbf{x})\, d^2\mathbf{x} \tag{1}$$

However, we can compute multiple frequencies simultaneously by Fourier-transforming the response to a short pulse, which is allowed in time domain methods [3]. We will accumulate the Fourier transforms $\mathbf{E}_\omega(\mathbf{x})$ and $\mathbf{H}_\omega(\mathbf{x})$ for every point in the flux plane via summation over the discrete time steps n,

$$\begin{aligned} \tilde{f}(\omega) &= \frac{1}{\sqrt{2\pi}} \sum_n e^{i\omega n \Delta t} f(n\Delta t)\Delta t \\ &\approx \frac{1}{\sqrt{2\pi}} \int e^{i\omega t} f(t) dt \end{aligned} \tag{2}$$

and compute $P(\omega)$ afterwards by the flux of these Fourier-transformed fields.

III. EXPERIMENTAL

We will simulate a two-dimensional PC, which will consist of an array of silicon nanopillars ($\varepsilon_r = 12$) embedded in air ($\varepsilon_r = 1$) distributed in an hexagonal lattice of 7×7 cells. Our simluations will be performed by studying different configurations of radii (r) and pitch (p). Our hexagonal lattice will be therefore described with Eq. (3).

$$\begin{aligned} \vec{a_1} &= p\hat{x} \\ \vec{a_2} &= \frac{p}{2}\left(\hat{x} + \sqrt{3}\hat{y}\right) \end{aligned} \tag{3}$$

To run our simulations we will use *Meep* [4], a free and open-source package which can solve Maxwell's equations by the FDTD method. The method requires a computational domain called cell, in which space will be discretized in a grid defined by a certain resolution. We need to make sure that we can solve the operating fields

*Electronic address: zoilo.nl@outlook.com

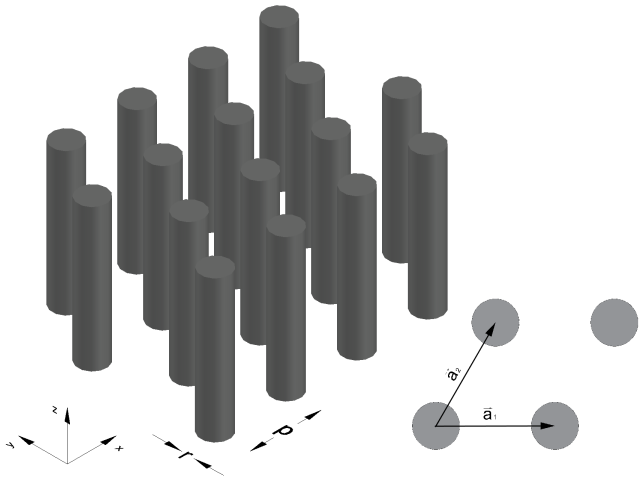

FIG. 1: Characterization of the structure, an hexagonal lattice of rods in air with an arbitrary length with every relevant parameter.

with enough precision; therefore, the length scale of the grid must be smaller than the propagation wavelength in the lossless dielectric material with the highest refractive index. It is recomended to have at least 8 pixels per wavelength [4]. Since we will be covering the 380-2500nm range, $\lambda = \lambda_0/\sqrt{\varepsilon_r \mu_r}$, where $\mu_r \approx 1$ will give us $\lambda_{silicon} \approx 109nm$ for the shortest wavelength we will compute. Accordingly, we will achive this by imposing a resolution of 80 pixels/μm.

The cell will contain all relevant objects for the simulation, such as the photonic crystal itself, which will be geometrized by introducing cilindrical objects of radius r with dielectric constant $\varepsilon_r = 12$ perpendicular to the x-y plane following Eq. (3) as shown in Fig. (1). For the entire part of the simulation we will restrict it to the x-y plane, using 3D vectors with z component equal to zero.

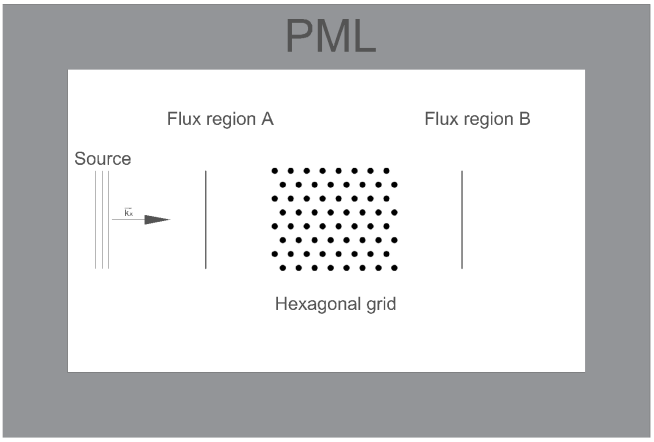

FIG. 2: Simulation setup with every relevant object.

The current source will be a Gaussian-pulse source, which unlike continuous sources, produces L^2 (square-integrable) fields, whose Fourier transform would otherwise be arbitrarily defined by the run time $n\Delta t$ of the simulation. Under these conditions, we are expecting a complete bandgap [5]. Therefore, we can arbitrarily set the source radiating in any direction within the x-y plane, $k_\parallel$. In our case we will set it in the x direction $k_\parallel = k\hat{x}$ as shown in Fig. (2). Since we will be using a high dielectric material concentrated in pillars in an hexagonal lattice filled with air, which makes the dielectric contrast strong, we also expect the bandgap to be TM-like [6]. Thus, the source must have its electric field polarized along the z direction, E_z, parallel to the axis of the rods.

Furthermore, for the correct simulation we need to ensure the convergence of the fields. For this reason we will provide enough simulation time steps n in Eq. (2), by setting a condition in which the fields have decayed enough before the simulation stops. In our case, $|E_z|^2$ must be 10^{-9} times its peak value at a given point, chosen in this simulation in the midle of the plane in which the transmission spectrum is computed.

Moreover, we will set where the flux will be computed by defining a flux region, a plane normal to the wave propagation before and after the photonic crystal so that we can calculate transmittance and reflectance spectra by computing the ratio of incident and transmitted power $P(\omega)$. Two flux regions will be used, one to calculate both the incident power for normalization and the reflected power (A), and another one to calculate the transmitted power though the crystal (B) as shown in Fig. (2).

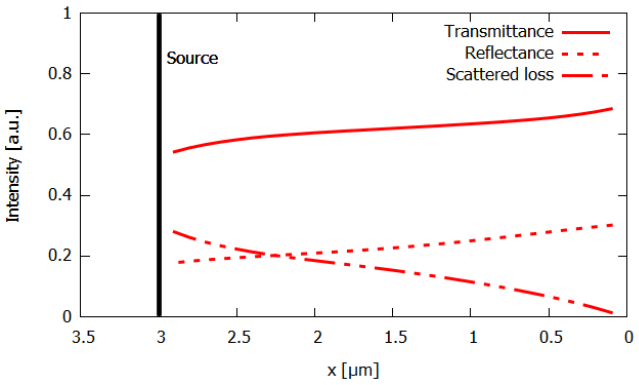

FIG. 3: Given a fixed source, the loss grows monotonically as the flux region strays a distance x from the PC. The figure shows the behavior for $\lambda = 2500nm$, the largest computed wavelength.

The current source will be fixed not too close to the grid, this is, the local density of states is affected by the sourrounding geometry, hence producing different fields [7]. The flux region, as we can see in Fig. (3) the farther away is set, higher scattered loss is computed. For this reason we will place our flux region 0.5μm away from both sides of the grid. Accordingly, the source will be placed at 1μm from the grid.

Since we are working with finite-sized cells, we must provide boundary conditions in order to prevent reflec-

tions. We achieve this by introducing a perfectly matched layer (PML) which is not properly a boundary condition but a virtual medium that absorbs electromagnetic waves at any incident angle or frequency [8]. However, the FDTD implementation of this layer produces numerical reflections which can be partially avoided by giving it a thickness more than half of the largest wavelength studied [3], in our case about 2μm.

IV. RESULTS

The PC presents a huge drop in the transmittance spectra in the near-infrared region as shown in Fig. (4). This decay plus high reflectance in the same region without appreciable loss can be correlated to the presence of a photonic band gap. Besides, we can see strong oscillations, especially at high wavelength regions, caused by interference effects and due to the small value of the silicon extinction coefficient in that range [2].

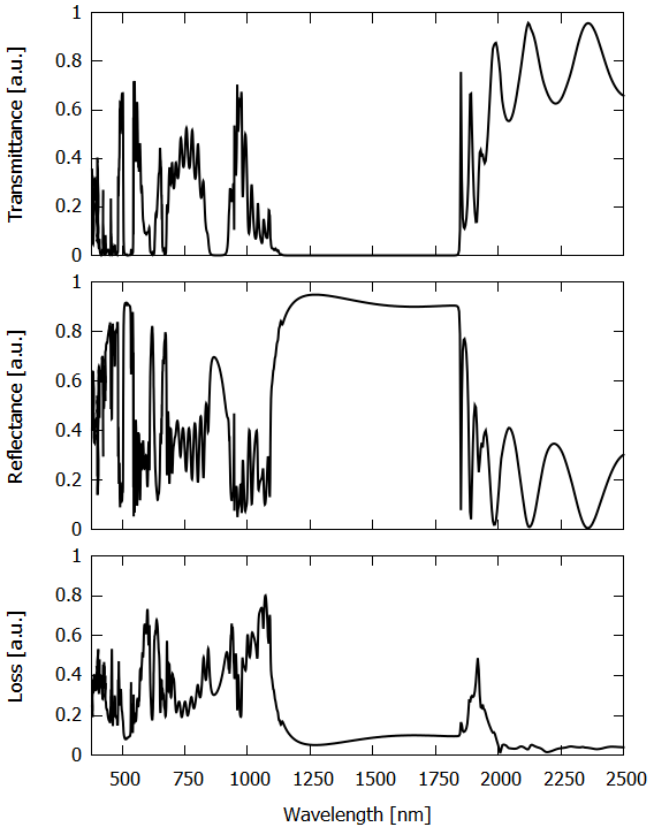

FIG. 4: Transmittance, reflectance and loss spectra of a PC with p=500nm and r=100nm.

In low wavelegths, the interference effect is smaller, but the loss grows as shown in Fig. (4). The simluation also suggests the presence of a secondary band gap around $\lambda = 900nm$, but has no real meaning as it is known that silicon is opaque at this wavelengths. We will study the dependece of these features as a function of different parameters such as radius and pitch.

A. Radius and pitch dependence

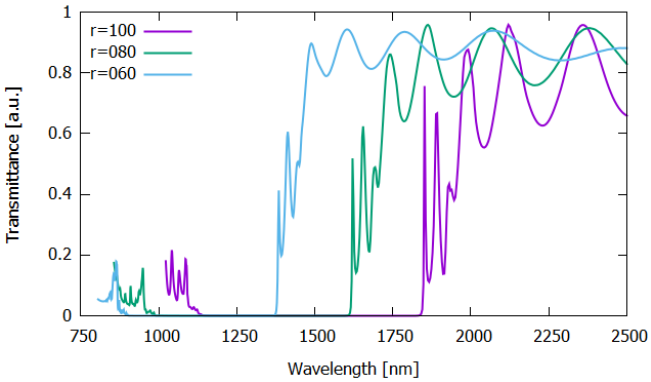

FIG. 5: Transmittance spectra of PCs with p=500nm given different radii for the silicon nanopillars.

We observe in Fig. (5) how the photonic bandgap width increases and its position redshifts when the nanopillar radius is increased. Besides, the oscillations at high wavelengths also vary, as they become sharper with the increasing radius. We could proceed in a similar manner with the pitch. However, since Maxwell equations are scalable [5], we shall calculate the gap-to-midgap ratio instead, $\Delta\lambda/\lambda_m$, which is scale independent, and compare photonic crystals using their radius-to-pitch ratio (r/p). We calculate then the spectra obtained combining 3 different radii and pitch, r={60,80,100}nm and p={300,400,500}nm respectively giving rise to 9 different combinations, 3 of whom mantain the same r/p ratio.

p [nm]	r [nm]	r/p	$\Delta\lambda$ [nm]	λ_m [nm]	$\Delta\lambda/\lambda_m$ [%]
300	60	0.20	410	905	45.30
300	80	0.26	440	1060	41.15
300	100	0.33	360	1250	28.80
400	60	0.15	480	1000	48.00
400	80	0.20	550	1195	46.02
400	100	0.25	610	1355	45.01
500	60	0.12	510	1125	45.33
500	80	0.16	650	1285	50.58
500	100	0.20	710	1485	47.81

TABLE I: Bandgap dimensions compared in various PC configurations.

As we see in the summary of the results presented in Table I, all 3 configurations with $r/p = 0.2$ have a roughly $46 \pm 2\%$ gap-to-midgap ratio, confirming the scalability stated before. Therefore, we can derive the central position λ_m, and width $\Delta\lambda$, of a band gap within a same r/p ratio by calculating new wavelengths as $\lambda' = \lambda \cdot s$, where s is the scaling factor. Comparing results for $r/p = 0.2$ obtained measuring directly on the spectra and computing them by scaling from the smallest radius, the results show a discrepancy less than 4%, which is acceptable

considering we are using a numerical method with finite resolution.

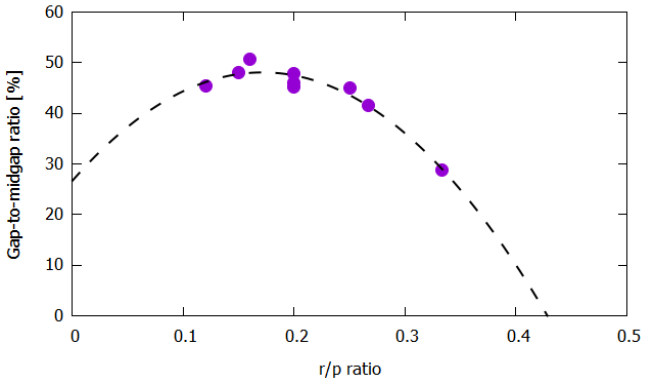

FIG. 6: Gap-to-midgap ratio dependence with r/p expressed in terms of %.

Fig. (6) shows that the dependance is non-linear. As we mentioned above, since the properties of photonic crystals are scalable we can easily explain why the bandgap redshifted in Fig. (5). Wavelength scales as $\sqrt{\varepsilon}$ [5], so increasing r increases the average dielectric constant of that medium, hence the photonic band gap is located at a higher wavelength. Also related, this could explain the behaviour at high wavelengths: the larger r is, stronger the interference effect, and thus, sharper the oscillations. Besides, the most interesting fact shown in Fig. (6) is the presence of an optimal r/p ratio in which the gap-to-midgap ratio is maximum for a given lattice geometry and dielectric contrast. In our case we find that the maximum appears at $r/p \approx 0.17$ with a value of 49%, in agreement with other works [5, 9]. This is why even being correct in our explanation about why bandgap position shifted, bandgap width, in absolute value, might increase or decrease in extreme cases where r/p is too high or low [6], contrarily to the trend shown in Fig. (5). That is why in all our simulations the badgap absolute size increases when increasing both radius and/or pitch, but not in the case $p = 300nm$ and $r = 100nm$, where it decreases compared to $p = 300nm$ and $r = 80nm$. In this particular case we have a $r/p = 0.33$, the highest ratio in our simulations, meaning that 40.3% of the volume is silicon. This is, at $r = 0.5p$ rods begin touching each other hindering the creation of TM modes, so the decrease in band gap width towards this region should be expected.

B. Defects

In this section we introduce defects in the structure and we compare the results with the ideal PC. In these simulations though, we will narrow the size of the source and flux regions to match the waveguide produced. This will help us highlighting new features easier since computing the spectra for a wider flux region would diminish their contribution because the normalization through the plane would be larger.

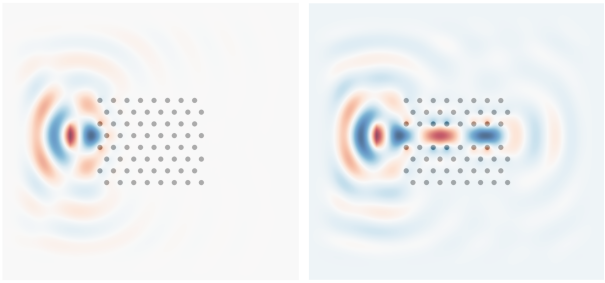

(a) (b)

FIG. 7: Side by side comparison of the electric field distribution in a perfect PC (a) and a modified PC (b) in which a complete row of pillars has been removed.

The first approach to a defect is shown in Fig. (7), where we compare the ideal PC we have worked with before with a new one in which a line defect is added by removing one row of pillars in the x direction. The figure shows the electric field for light propagation through the PC for $\lambda = 1.40\mu m$ which is within the bandgap. Fig. (7a) shows how the propagation is neglected, while Fig. (7b) shows how light is confined and guided through the defect. This is, the photonic bandgap of the surrounding crystal guides the light in the air forbidding its propagation in any other direction. Removing several rows can produce multi-mode waveguides, which are undesirable for information transmission purposes [5]. For this reason our simulations will stick with only one row.

Additionally, we can introduce point defects, which will perturbate the translational symmetry of the lattice, creating single modes at wavelengths within the bandgap. A point defect can be intruduced in several ways, either changing the dielectric constant of a single rod, its radius, or eliminating one of them creating a cavity.

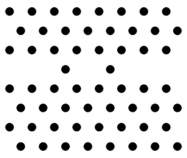

FIG. 8: Nanopillar distribution for a narrow-band filter device.

However, since we want to be operating inside the bandgap, we will produce a waveguide to the cavity, removing all nanopillars but two, as shown in Fig. (8). Light is then guided through an input waveguide and coupled inside the cavity, which produces a resonance, thus light is coupled again into an output waveguide as shown in Fig. (9). Analyzing the transmission spectra we find the sharp resonance peak inside the gap at $\lambda = 1.28\mu m$

as shown in Fig. (10). By this we obtain a narrow-band filter, a device capable of transmit light at frequencies within the bandgap near the resonant frequency of the cavity.

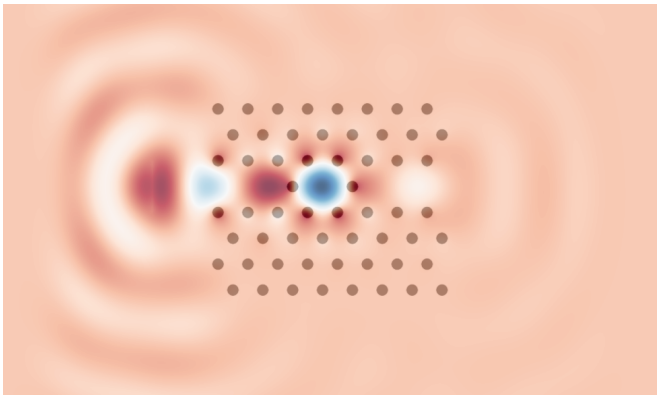

FIG. 9: Electric field transmission for the resonant wavelength $\lambda = 1.28\mu m$.

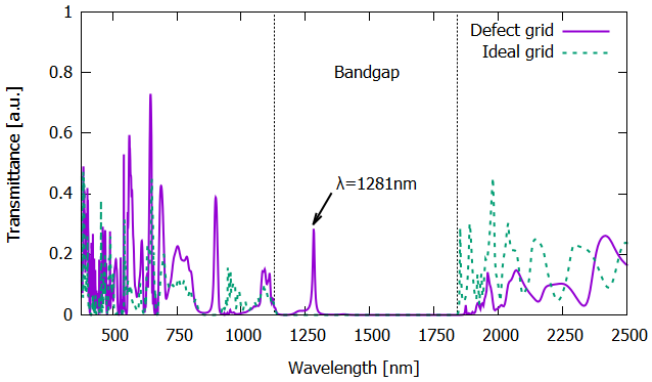

FIG. 10: Transmittance spectra of a PC with pitch=500nm and radius=100 with and without the introduced defect.

V. CONCLUSIONS

The simulation process proved to be a powerful tool in the designing procedure of photonic crystal based devices, allowing reliable tests for bandgap usability.

We have concluded that the bandgap width is not function of the radius and pitch separately, but function of an overall filling ratio, which can be expressed in terms of r/p. This bandgap has proven to be scalable which enforces the idea that it depends on the concentration of dielectric materials nor lattice dimensions.

A maximal gap-to-midgap width is found at $r/p = 0.17$ for the silicon based nanopillars in an hexagonal lattice.

The presence of these bandgaps allow to design waveguides, consisting in the removal of one row of pillars, and filters based on cavities, constisting of two rods in a waveguide. For this later structure, in the case $p = 500nm$ and $r = 100nm$, a resonance peak is found at $\lambda = 1.28\mu m$.

Acknowledgments

I would like to thank my advisor, Albert Romano Rodriguez for introducing me to this field and providing me a different point of view about physics. I also want to express my gratitude to my co-advisor Elena López Aymerich, for her always positive attitude towards me and her willingness to help. Last but not least, special thanks to my family for their unconditional support and my classmates for helping me with some tweaks in the process.

[1] P. R. Villeneuve, S. Fan, and J. D. Joannopoulos. "Microcavities in photonic crystals: Mode symmetry, tunability, and coupling efficiency", *Phys. Rev. B.*, vol. 54, pp. 7837-7842, 1996.

[2] L. Hu and G. Chen. "Analysis of Optical Absorption in Silicon Nanowire Arrays for Photovoltaic Applications", *Nano Letters*, vol. 7, pp. 3249-3252, 2007.

[3] A. Taflove and S. C. Hagness, *Computational Electrodynamics: The Finite-Difference Time-Domain Method*, (Artech House, 2005, 3rd. ed.).

[4] *http://ab-initio.mit.edu/meep* (Last visited 11/06/2019)

[5] J. D. Joannopoulos, S. G. Johnson, J. N. Winn and R. D. Meade. *Photonic Crystals: Molding the Flow of Light*, (Princeton University Press, 2008, 2nd. ed.).

[6] S. G. Johnson, S. Fan, P. R. Villeneuve, J. D. Joannopoulos and L. A. Kolodziejski. "Guide modes in photonic crystal slabs", *Phys. Rev. B.*, vol. 60, pp. 5751-5758, 1999.

[7] A. Taflove, A. Oskooi and S. G. Johnson. *Advances in FDTD Computational Electrodynamics: Photonics and Nanotechnology*, (Artech House, 2013).

[8] J.P. Bérenger. "A perfectly matched layer for the absorption of electromagnetic waves", *J. Comput. Phys.*, vol. 114, pp. 185–200, 1994.

[9] B. Jiang, A. Liu, W. Chen, M. Xing, W. Wenjun and W. Zheng. "The optimization of large gap–midgap ratio photonic crystal with improved Bisection-Particle Swarm Optimization", *Opt. Commun.*, vol. 284, pp. 226-230, 2011.